Necessity of Hydrostatic Stability in Autonomous Underwater Vehicles on Intervention Missions

Tobias Rossol* , Christian Ernst Siegfried Koch* , Ralf Bachmayer† , Frank Kirchner*‡
*German Research Center for Artificial Intelligence (DFKI)
Bremen, Germany
{first_name.surname}@dfki.de
†MARUM - Center for Marine Environmental Sciences
University of Bremen
Bremen, Germany
rbachmayer@marum.de
‡University of Bremen, Dep. Mathematics & Computer Science
Bremen, Germany
frank.kirchner@informatik.uni-bremen.de

***Abstract*—Most underwater vehicles are hydrostatically stable, i.e., their center of gravity is placed below their center of buoyancy, providing passive stability in pitch and roll. While this design is favorable for fixed attitude missions, it is a hindrance for tasks requiring flexible orientation control. This work examines the influence of hydrostatics on attitude control of a fully actuated intervention type Autonomous Underwater Vehicle (AUV). We conducted a simulation study varying influencing factors, such as hydrostatic stability, thruster dynamics, disturbance, and controller choice. We found that the impact of hydrostatic stability on control performance and energy consumption is drastically reduced, if thrusters with sufficiently high dynamic range are used. Our results support the concept of intervention AUVs, which are highly agile through marginally stable design.**

***Index Terms*—autonomous underwater vehicle, hydrostatic stability, attitude control, thruster model, hydrobatics**

I. Introduction

Autonomous underwater intervention has been an active research field for decades and is still considered a challenge in underwater robotics with diverse areas of application [1]. To cope with a preferably large range of potential manipulation tasks, it seems advantageous to provide an Intervention AUV (I-AUV) with a high maneuverability in pitch and roll: the manipulator and equipment as cameras and light can be directly pointed to the object of interest regardless of the target's position in space (e.g. on the seafloor or even overhead in some underwater facility); easier navigation through narrow environments like caves; potential decrease of manipulator complexity by leveraging the vehicle's Degrees of Freedom (DOF).

As most underwater vehicles, I-AUVs are usually designed hydrostatically stable by placing their Center of Gravity (CG) under their Center of Buoyancy (CB) (e.g. [2]), as shown in Fig. 1a. Thereby, the vehicle is passively stable against disturbances in pitch and roll, due to self-righting moments. However, concerning maneuverability beyond yaw control, high thruster power is needed to achieve attitudes other than the stable one. An alternative design approach is what we refer to as hydrostatic orientation control and is common for underwater gliders (see e.g. [3]). By actively shifting the CG and/or CB through relocation of vehicle mass and/or volume, the stable attitude can be defined as desired (Fig. 1c). The drawback of this method is that potentially high masses or volumes have to be moved. Another design paradigm is to place the CG and CB as close to each other as possible (Fig. 1b). Since the vehicle is only marginally stable in this case, it can be orientated as desired, but passive stability is lost. Of course, achieving perfect marginal stability is not possible in praxis. However, if CG and CB are sufficiently close, the restoring moments are negligible compared to actuation and disturbances.

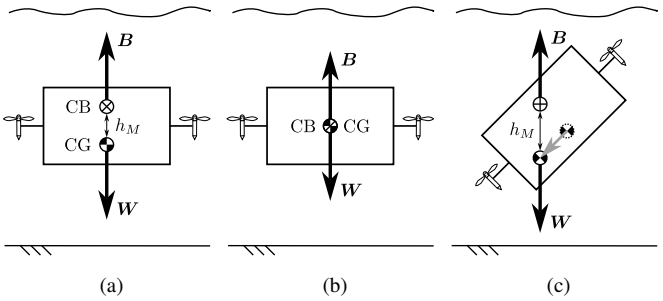

Fig. 1. Hydrostatic configurations. (a): Hydrostatically stable; (b): Marginally stable; (c): Hydrostatic orientation control. $\boldsymbol{B}$ is buoyancy, $\boldsymbol{W}$ is weight and h_M denotes the metacentric height, which is the distance between Center of Gravity (CG) and Center of Buoyancy (CB) and therefore is a measure for hydrostatic stability.

Recently, the term *hydrobatics* emerged, refering to agile maneuvering underwater vehicles [4]. Two examples for hydrobatic vehicles in the context of research are

The work decribed in this paper has received funding by the German Federal Ministry of Education and Research (grant no. 01IS17029A) as well as the Federal Ministry of Economic Affairs and Climate Action (grant no. 03SX540D).

HippoCampus [5], a low-cost micro AUV, and the *MIT Omnidirectional Submersible* [6], a spherical robot designed for nuclear reactor inspection. With the *Ocean Module V8* range [7], hydrobatics also gained traction in commercially available Remotely Operated Vehicles (ROVs). To achieve high maneuverability, the vehicles mentioned here are designed to have a small metacentric height, i.e., the distance between CG and CB is close, and can be characterized as hydrostatically marginally stable.

In contrast to state of the art I-AUVs, the novel robot *Cuttlefish* [8] (Fig. 2a) is designed to freely assume any orientation in the water column during the interaction with the environment or the manipulation of objects. Towards this goal, *Cuttlefish* is equipped with a movable mass enabling the switch from a hydrostatically stable configuration towards a marginally stable configuration. Furthermore, *Cuttlefish* is fully actuated with eight thrusters to control its orientation in the presence of disturbances, e.g., currents and coupling forces during the manipulation.

Our work is primarily motivated by the question if the loss of passive stability in a marginally stable I-AUV can be compensated by full actuation and adequate attitude control. Related work considering hydrostatic stability has focused on stability properties of AUV motion [9], [10] or on motion performance of torpedo-shaped AUVs [11]. We are not aware of any research concerning the influence of hydrostatic stability on control performance and energy consumption of slow moving or hovering, box-shaped vehicles.

The paper is structured as follows. Section II investigates the effect of hydrostatics on stability of pitch control. In Section III we present a simulation study that examines the influence of hydrostatic stability on control performance and energy consumption. The remaining part of the paper discusses the obtained results and outlines the conclusions we drew from our findings.

II. Stability Analysis

Since hydrostatics provide passive stability in the form of restoring forces, it would not be surprising if the lack of hydrostatic stability also affected the stability of motion of the overall system. We therefore used basic nonlinear stability theory to examine the influence of hydrostatic stability on the stability properties of the controlled closed loop system.

According to Fossen [12], the dynamics of an underwater vehicle can be described using the following vectorial notation:

$$\dot{\boldsymbol{\eta}} = \boldsymbol{J}_{\Theta}(\boldsymbol{\eta})\,\boldsymbol{v} \tag{1}$$

$$\boldsymbol{M}\dot{\boldsymbol{v}} + \boldsymbol{C}(\boldsymbol{v})\,\boldsymbol{v} + \boldsymbol{D}(\boldsymbol{v})\,\boldsymbol{v} + \boldsymbol{g}(\boldsymbol{\eta}) = \boldsymbol{\tau} \tag{2}$$

Equation (1) represents the kinematics; herein, $\boldsymbol{\eta} = [x, y, z, \phi, \Theta, \psi]^T$ is the pose (position and orientation) of the vehicle expressed in an earth-fixed coordinate system, while $\boldsymbol{v} = [u, v, w, p, q, r]^T$ is the linear and angular velocity of the vehicle relative to the earth-fixed frame expressed in a body-fixed coordinate system. For this work, the use of Euler angles is sufficient, though, for 6 DOF control alternative representations of orientation are usually required, as elaborated in [13]. In (2), $\boldsymbol{M} = \boldsymbol{M}_{RB} + \boldsymbol{M}_A$ is the inertia matrix accounting for both the mass and inertia of the rigid body ($\boldsymbol{M}_{RB}$), as well as the hydrodynamic added mass and inertia ($\boldsymbol{M}_A$). The matrix $\boldsymbol{C}(\boldsymbol{v})$ represents the Coriolis and centripetal forces and $\boldsymbol{D}(\boldsymbol{v})$ considers hydrodynamic damping effects. The hydrostatics are accounted for by $\boldsymbol{g}(\boldsymbol{\eta})$ and $\boldsymbol{\tau} = [X, Y, Z, K, M, N]^T$ includes the forces and moments acting on the vehicle.

To facilitate the subsequent analysis, we focused on motion in only one of the DOF that are directly affected by hydrostatic stability, in our case pitch. We presumed that the vehicle is symmetric in three planes and is only actuated and disturbed in pitch. We further assumed that remaining coupling terms in $\boldsymbol{C}(\boldsymbol{v})$ are comparatively small and that hydrodynamic damping can be adequately modeled with a linear (d_l) and a quadratic (d_q) damping term. Keeping in mind that $q = \dot{\Theta}$ holds in this simple one-dimensional case, we arrived at the 1 DOF model

$$M'\ddot{\Theta} + d_l\dot{\Theta} + d_q|\dot{\Theta}|\dot{\Theta} + Wh_M \sin\Theta = \tau_{th} + w. \tag{3}$$

The torque exerted on the vehicle is subdivided into the part of the thrusters τ_{th} and the part of the disturbance w. The combined inertia $M' = I_y - M_{\dot{q}}$ accounts for both rigid body (I_y) and added inertia ($M_{\dot{q}}$), W is the vehicle's weight and h_M is the metacentric height (distance between CG and CB).

For the thruster input we chose a simple nonlinear PD control law

$$\tau_{th} = -k_p(\Theta - \Theta_d) - k_d\dot{\Theta} + Wh_M \sin\Theta \tag{4}$$

where $k_p, k_d > 0$ are the proportional and differential gain, respectively, and Θ_d is the desired pitch angle.

The resulting vehicle system can be expressed in state-space form as:

$$\dot{\boldsymbol{x}} = \boldsymbol{f}(\boldsymbol{x}, \boldsymbol{u})$$

$$\begin{bmatrix}\dot{\Theta}\\ \ddot{\Theta}\end{bmatrix} = \begin{bmatrix}\dot{\Theta}\\ -\frac{1}{M'}\left(k_p\Theta_e + k_d\dot{\Theta} + d_l\dot{\Theta} + d_q|\dot{\Theta}|\dot{\Theta} - w\right)\end{bmatrix} \tag{5}$$

$$\text{where} \quad \Theta_e = \Theta - \Theta_d$$

Commanding a constant pitch angle of $\Theta_d = \overline{\Theta}_d$ in presence of a constant disturbance $w = \overline{w}$, the vehicle system (5) has one equilibrium point $\boldsymbol{x}_e = \left[\overline{\Theta}_d + \frac{\overline{w}}{k_p}, 0\right]^T$. Applying Lyapunov's direct method, it is possible to show that this equilibrium point is globally asymptotically stable. The derivation can be found in [14], it is based on a similar examination in [12]. According to our analysis, stable control is possible and the desired pitch angle can be achieved with a steady-state error of $\frac{\overline{w}}{k_p}$, which will diminish after the disturbance has fully vanished.

What is striking is that this result is independent of hydrostatic stability, since hydrostatics are cancelled out in the control law (4). Due to the lack of integrator action, (4) leaves a steady state error in presence of a disturbance. More sophisticated control laws are presented in section III-D.

From the analysis in this section we conclude that hydrostatic stability is not a strict necessity for stable pitch control.

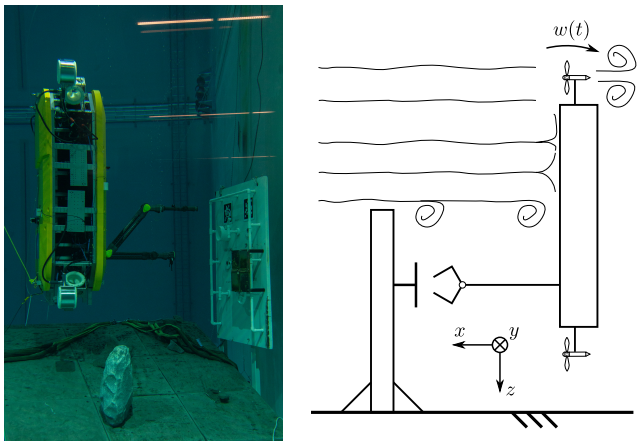

(a) (b)

Fig. 2. (a): *Cuttlefish* in manipulation pose. (Photo: Thomas Frank, DFKI) (b): Illustration of simulation scenario.

TABLE I
SIMULATION STUDY FACTORS AND FACTOR LEVELS

Factor	number of levels	levels
Metacentric height	7	$-1\,\text{cm}$, $0\,\text{cm}$, $1\,\text{cm}$, $5\,\text{cm}$, $10\,\text{cm}$, $20\,\text{cm}$, $30\,\text{cm}$
Thruster dynamics	2	High and low power thrusters
Disturbance signal	5	$100\,\text{N m}$-step, $500\,\text{N m}$-step, $1000\,\text{N m}$-step, random signal #1, random signal #2
Controller	2	PID control, LQR control

III. SIMULATION OF AUV MOTION

The analytical analysis in the previous section indicated that an underwater vehicle does not necessarily need to be hydrostatically stable to achieve stable control. Though, it did not reveal if hydrostatic stability has any effect on control performance or energy consumption. To tackle this question, we conducted a simulation study.

A. Scenario and Study Design

The simulation scenario (Fig. 2b) is inspired by a situation potentially encountered by *Cuttlefish*. In preparation for a manipulation task, the vehicle is hovering in front of an underwater facility where it is perturbed by currents. The goal of the controller is now to keep the vehicle's orientation to provide a stable base for the manipulator. The scenario is assumed to be symmetrical to the xz-plane and the disturbance is considered to occur only as a torque $w(t)$ around the y-axis. Consequently, this examination again focuses on the DOF pitch.

In our study, we varied the influencing factors metacentric height, thruster dynamics, disturbance, and controller choice, as shown in Table I. As a measure for hydrostatic stability, we let the metacentric height range from slightly unstable to a value we considered as slightly greater than realistic for *Cuttlefish*. The levels are spaced unevenly, because preliminary simulations indicated greater variance close to marginal stability. As disturbances we chose step signals to three different amplitudes and two random signals created from the same random seed, with the second signal having twice the energy (major part located in the frequency band below $1\,\text{Hz}$) of the first one. The factors thruster dynamics and controller will be described in more detail below. For the study, we chose a full factorial design; i.e., every possible combination of factor levels was examined, resulting in a total number of 140 simulations.

In our study, the responses of interest were control performance and energy consumption. For quantitative assessment, we selected the following metrics: The Integral of Squared Error (ISE) and the Integral of Absolute Error (IAE) served as a measure for control performance. We additionally included the maximum absolute pitch angle $\Theta_{\max}$ as a more intuitively interpretable value. Energy consumption was considered by the average power $\overline{P}$ required by the thrusters. The metrics were calculated according to

$$\text{ISE} = \int_0^T \left(e\left(t\right)\right)^2 dt \tag{6}$$

$$\text{IAE} = \int_0^T \left|e\left(t\right)\right| dt \tag{7}$$

$$\Theta_{\max} = \max\left(\left|\Theta\left(t\right)\right|\right) \tag{8}$$

$$\overline{P} = \frac{1}{T}\int_0^T P\left(t\right) dt \tag{9}$$

where e is the control error, $\max(\cdot)$ is the maximum norm, $P(t)$ is the power consumed by the thrusters (calculated from static manufacturer data) and T is the simulation time. The latter was selected such that the controller was able to suppress the disturbance effectively or was set to $60\,\text{s}$ for the random disturbances. Simulation time was the same throughout comparison of different metacentric heights in a specific set of the other factor levels.

Simulations started at a pitch angle of $\Theta = 0°$, which was the hydrostatically stable attitude. Then, a disturbance was applied and the controller was commanded to keep the stable pitch angle of $0°$. During simulation, the metrics were calculated.

The simulation study was conducted using *Simulink* from *The MathWorks, Inc*. A schematic overview of the implemented simulation model is given in Fig. 3; its individual components will be described subsequently.

B. Vehicle Model

Although the simulation study focused on pitch only, we implemented a 3 DOF vehicle model to allow for potential future expansions and to verify that the effect of remaining coupling terms is small (which was the case). Since *Cuttlefish* is approximately port-starboard symmetric, we used a longitudinal subsystem, which accounts for the DOF surge, heave and pitch.

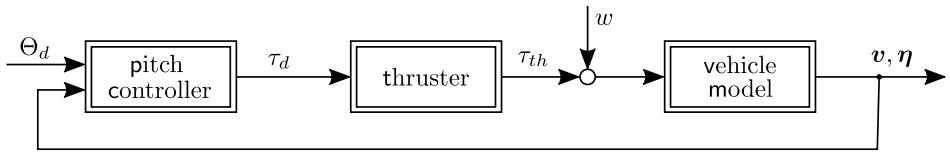

Fig. 3. Overview of implemented simulation model.

According to [12], the off-diagonal elements of the added mass and inertia matrix $\boldsymbol{M}_A$ are comparatively small. Neglecting these terms we obtained the inertia matrix as:

$$\boldsymbol{M} = \begin{bmatrix} m - X_{\dot{u}} & 0 & m z_g \\ 0 & m - Z_{\dot{w}} & -m x_g \\ m z_g & -m x_g & I_y - M_{\dot{q}} \end{bmatrix} \tag{10}$$

Herein, $X_{\dot{u}}$, $Z_{\dot{w}}$ and $M_{\dot{q}}$ are the remaining diagonal added mass and inertia terms, m is the vehicle mass and x_g and z_g denote the CG position relative to the body-fixed x- and z-axis, respectively. Assuming all movements and forces concerning sway, roll and yaw to be zero, we parameterized the Coriolis and centripetal matrix as:

$$\begin{aligned} \boldsymbol{C}(\boldsymbol{v}) = &\begin{bmatrix} 0 & 0 & (m - Z_{\dot{w}})\, w \\ 0 & 0 & -(m - X_{\dot{u}})\, u \\ -(m - Z_{\dot{w}})\, w & (m - X_{\dot{u}})\, u & 0 \end{bmatrix} \\ &+ \begin{bmatrix} 0 & 0 & -m x_g q \\ 0 & 0 & -m z_g q \\ m x_g q & m z_g q & 0 \end{bmatrix} \end{aligned} \tag{11}$$

Hydrodynamic damping was presumed to be decoupled and is accounted for by linear (X_u, Z_w, M_q) and quadratic ($X_{|u|u}$, $Z_{|w|w}$, $M_{|q|q}$) terms:

$$\begin{aligned} \boldsymbol{D}(\boldsymbol{v}) = &\operatorname{diag}\left\{-X_u, \quad -Z_w, \quad -M_q\right\} \\ &+ \operatorname{diag}\left\{-X_{|u|u}|u|, \quad -Z_{|w|w}|w|, \quad -M_{|q|q}|q|\right\} \end{aligned} \tag{12}$$

The vehicle was considered as neutrally buoyant and CB and CG were presumed to lie on the port-starboard symmetry plane. The hydrostatics thus become:

$$\boldsymbol{g}(\boldsymbol{\eta}) = \begin{bmatrix} 0 \\ 0 \\ W h_M \sin(\Theta) + W(x_g - x_b)\cos(\Theta) \end{bmatrix} \tag{13}$$
$$\text{with} \quad h_M = z_g - z_b$$

Throughout the simulation study, the origin of the body-fixed reference frame coincided with CB and CG was positioned on the vehicle's z-axis. In this case, $x_g = x_b = z_b = 0$ holds.

For implementation in *Simulink*, the equations of motion (2) were rearranged as:

$$\dot{\boldsymbol{v}} = \boldsymbol{M}^{-1}\left[\boldsymbol{\tau} - \left[\left(\boldsymbol{C}(\boldsymbol{v}) + \boldsymbol{D}(\boldsymbol{v})\right)\boldsymbol{v} + \boldsymbol{g}(\boldsymbol{\eta})\right]\right] \tag{14}$$

In the appendix, Table III summarizes the vehicle model parameters that we used throughout our simulations.

TABLE II
SPECIFICATIONS OF THRUSTER REFERENCES

Thruster	max. thrust forw./rev. [N]	power at max. thrust [W]	outer ∅ [mm]	weight (air) [kg]
Blue Robotics T200 (@ 16 V) [15]	51.5/40.2	390	100	0.34
TSL Technologies 150 mm IntegratedThruster [16]	237/237	1000	208	7.7

C. Thruster Model

Since we expected thruster dynamics to have a noticeable effect on study outcome, we compared two different types of thrusters. To ensure realistic presumptions made for simulation, we used two commercially available thrusters as real-world references: the *Blue Robotics* T200 as a small-sized and comparatively fast thruster, and the *TSL Technologies* 150 mm *IntegratedThruster* as a larger-sized high power thruster with a slower response time. Specifications are compared in Table II. Throughout the following sections, we refer to the compared thrusters in a more general way as the "Low Power" (LP) and the "High Power" (HP) thrusters.

To represent the thrusters in simulation, we started with the model for torque-controlled thrusters by Yoerger et al. [17]. Since the model dynamics did not agree well with experimental data, we assumed the considered thrusters to be speed-controlled, though we could not find sufficient information about the control schemes actually implemented on the driver electronics.

For our study, we extended Yoerger's model [17] with a speed control loop, as shown in Fig. 4: The first block discretizes the thrust command and thereby represents the maximum update frequency of the thruster electronics. The "low RPM behavior" block accounts for the fact that the thrusters require a minimum speed to work properly. Any commands violating this constraint are dropped to zero. The remaining core of the model can be described by the following set of equations:

$$e = \frac{T_d}{C_t} - \Omega|\Omega| \tag{15}$$

$$\tau' = Pe + Ih \tag{16}$$

$$\tau_s = \max\left(\min\left(\tau', \tau_{\max}\right), \tau_{\min}\right) \tag{17}$$

$$\dot{h} = \begin{cases} 0 & \text{if} \quad \tau_s = \tau_{\max} \quad \text{and} \quad \operatorname{sgn}(e) = \operatorname{sgn}(h) \\ 0 & \text{if} \quad \tau_s = \tau_{\min} \quad \text{and} \quad \operatorname{sgn}(e) = \operatorname{sgn}(h) \\ e & \text{else} \end{cases} \tag{18}$$

$$\dot{\Omega} = \beta\tau_s - \alpha\Omega|\Omega| \tag{19}$$

$$T = C_t\Omega|\Omega| \tag{20}$$

where T_d denotes the desired thrust, Ω the propeller angular velocity and C_t is a proportionality constant. The speed control error e is introduced as a helping variable as well as τ', which is the result of the control law equation. Herein, P and I denote the proportional and integral gain of the controller, respectively, and h is the state of the controller's integrator. Equation (17) ensures that the controller output stays within its limits of $\tau_{\min}$ and $\tau_{\max}$. In (18), a simple anti-windup algorithm is realized. Integration is stopped when the controller limits are reached and control error e and integrator output h are of the same sign. Equations (19) and (20) basically describe the original model of Yoerger et al. [17], where τ_s is the propeller shaft torque, α and β are constant model parameters and T is the generated thrust. The values we used as thruster model parameters are presented in Table IV.

Note that our thruster model is an empirical description of the input-output dynamics of thrust generation of a system consisting of thruster and control electronics. It is beyond the scope of this model to provide any insights into the internal thruster dynamics.

As can be seen in Fig. 6 and Fig. 7, model response is in good agreement with experimental data for the *Blue Robotics* T200 thruster. Furthermore, our model clearly outperforms a simpler approximation with a first order lag.

Experimental data were acquired using a simple low-cost test bench, shown in Fig. 5. Herein, the thruster is attached to a lever that transmits force to two compression load cells (*TE Connectivity* FX29K0-100A-0010-L), one for forward and one for reverse direction. The setup is of limited accuracy and transients of the test bench structure are apparent in the signal. While we considered the data as sufficient for model verification to the extent of our study's purposes, the data should be interpreted with caution.

Concerning the *TSL* $150\,\mathrm{mm}$ thruster, we had to rely on thrust reversal data recorded previous to our study. The used test bench suffered from hysteresis and thrust was only measured in one direction. Therefore, model fitting and verification turned out difficult. Though, we considered the result (Fig. 8) as sufficient to model the required rise time in thrust response.

Regarding thruster configuration, we presumed one *TSL* $150\,\mathrm{mm}$ thruster to be located at each corner of the vehicle with a lever of $1.2\,\mathrm{m}$ about the CG. For the scenarios using the T200 thrusters, each *TSL* thruster was replaced by six T200 devices.

D. Pitch Controller

To reduce bias concerning controller choice, we compared a cascaded PID control (Fig. 9) with a Linear Quadratic Regulator (LQR) approach (Fig. 10). The controllers' integrator outputs were all limited and featured anti-windup as used in the thruster model in (18). Both control schemes were combined with feedback linearization to enhance control performance. With the desired angular acceleration $\dot{q}_d$ as the controller output, the required thruster torque was calculated by:

$$\tau_{th} = (I_y - M_{\dot{q}})\,\dot{q}_d - M_q q - M_{|q|q}|q|q + W h_M \sin\Theta \tag{21}$$

In a perfect scenario, this allows the controller to directly command the angular acceleration as desired ($\dot{q} = \dot{q}_d$). Because feedback linearization is not exact in reality, we intentionally altered the model parameters in (21) to deviate from the vehicle model by plus or minus $20\,\%$. The controllers were tuned separately for the LP and the HP thrusters scenarios. Controller parameters are given in Tables V and VI.

E. Simulation Results

The results of our simulations are summarized in Fig. 11. To compare trends in data among the different disturbances, we scaled data such that all maximum values ($m_{j,\max}$) encountered equal one and the minimum values ($m_{j,\min}$) equal zero:

$$m^*_{i,j} = \frac{m_{i,j} - m_{j,\min}}{m_{j,\max} - m_{j,\min}} \tag{22}$$

where $m^*_{i,j}$ is the scaled datum, and $m_{i,j}$ is the original one. The index of the datum is i and j corresponds to the underlying disturbance. Since scaling lead to a loss of information about how much values changed, we additionally introduced the savings φ:

$$\varphi_{i,j} = \left(1 - \frac{m_{i,j}}{m_{j,h_M=0}}\right) \cdot 100\,\% \tag{23}$$

The savings describe how much of a particular metric was "saved" compared to the marginally stable configuration ($m_{j,h_M=0}$). As an example, in the first plot of the fourth row of Fig. 11: with a step-disturbance to $1000\,\mathrm{N\,m}$, at a metacentric height of $10\,\mathrm{cm}$, $94\,\%$ of ISE were saved, or alternatively the ISE was decreased by $94\,\%$, compared to the marginally stable configuration.

What stands out in Fig. 11 is the difference in outcome between HP and LP thrusters. For the HP thrusters, metric values decreased, i.e., improved in an exponential fashion when hydrostatic stability was raised. This decrease saturated when hydrostatic stability was further increased. This effect was stronger for larger disturbances. The savings φ reveal that improvement due to hydrostatic stability was strong, reaching values close to $100\,\%$. In contrast, metric values also decreased for the LP thrusters but with a linear trend and actual improvements comparatively weak with $\varphi < 9\,\%$.

The difference in control performance between LP and HP thrusters was also clearly present in the values for $\Theta_{\max}$, which were substantially lower for the LP thrusters. As an example, for the $500\,\mathrm{N\,m}$ step disturbance the lowest value encountered for the HP thrusters was $\Theta_{\max} = 11.9°$ (at

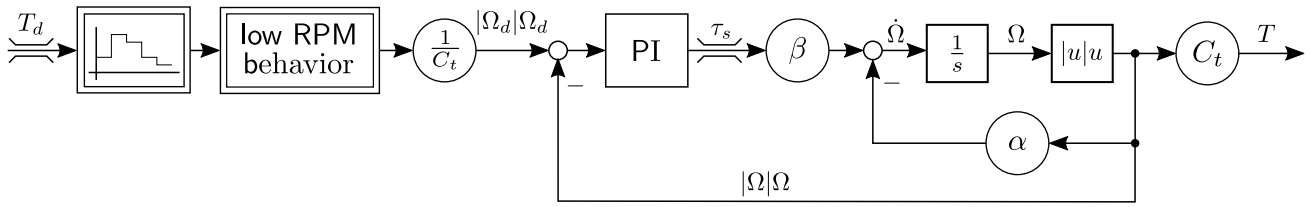

Fig. 4. Block diagram of thruster model implemented in simulation.

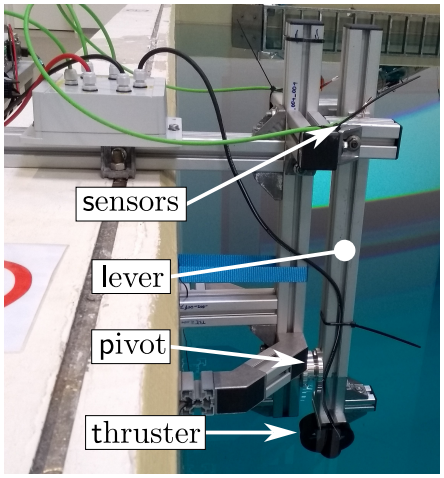

Fig. 5. Thruster test bench. The sensors are mounted opposed to each other, facing the lever. To prevent looseness between sensors and lever, the setup is preloaded at zero thrust. Loss of pretension and looseness in the bearings of the pivot are the main reasons why complete system accuracy is less than accuracy of the individual sensors. A more detailed description of the test bench and a closer examination of its performance can be found in [14].

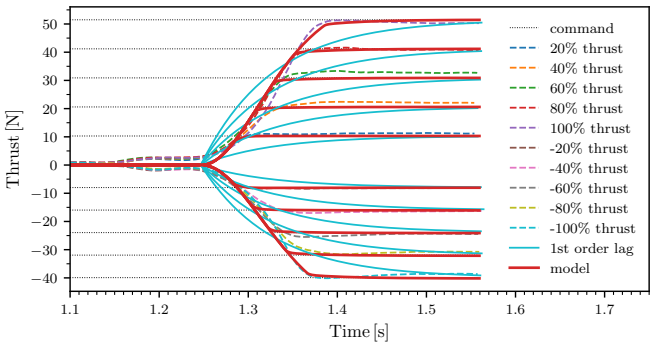

Fig. 6. Comparison of LP thruster model and first order lag step responses with experimental data of a *Blue Robotics* T200 thruster. Experimental data were low-pass filtered and averaged. When starting from standstill, the T200 device started to generate thrust after a delay of approximately 250 ms. Since this initial delay is not represented by our model, the responses of both the model and the first order lag were manually shifted in this figure. We considered this delay issue as negligible for our study, because standstill was only encountered in the beginning of each simulation.

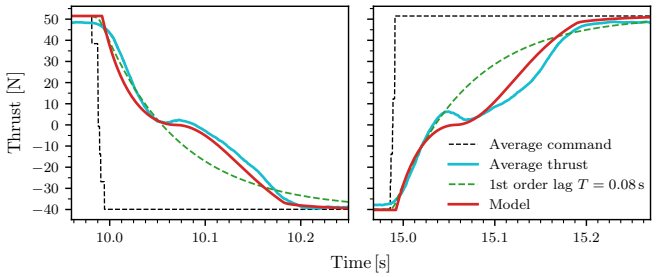

Fig. 7. Comparison of LP thruster model and first order lag thrust reversal with experimental data of a *Blue Robotics* T200 thruster. Experimental data were low-pass filtered and averaged.

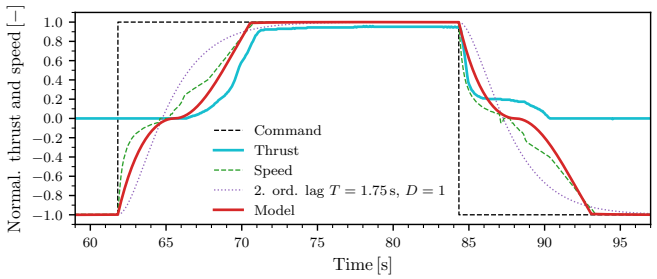

Fig. 8. Comparison of HP thruster model and second order lag thrust reversal with experimental data of a *TSL Technologies* 150 mm IntegratedThruster. Thruster speed was included in this figure to be suggestive of thruster behavior in the reverse direction, where thrust was not measured.

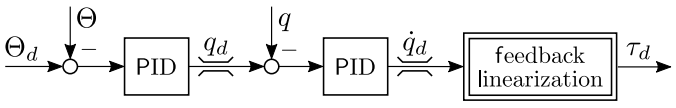

Fig. 9. Block diagram of cascaded PID pitch controller.

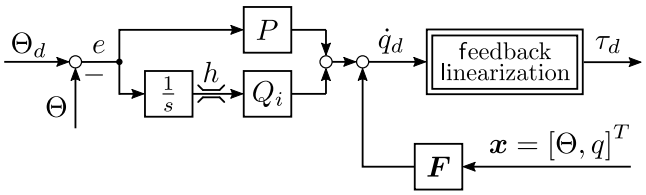

Fig. 10. Block diagram of LQR pitch control with PI structure.

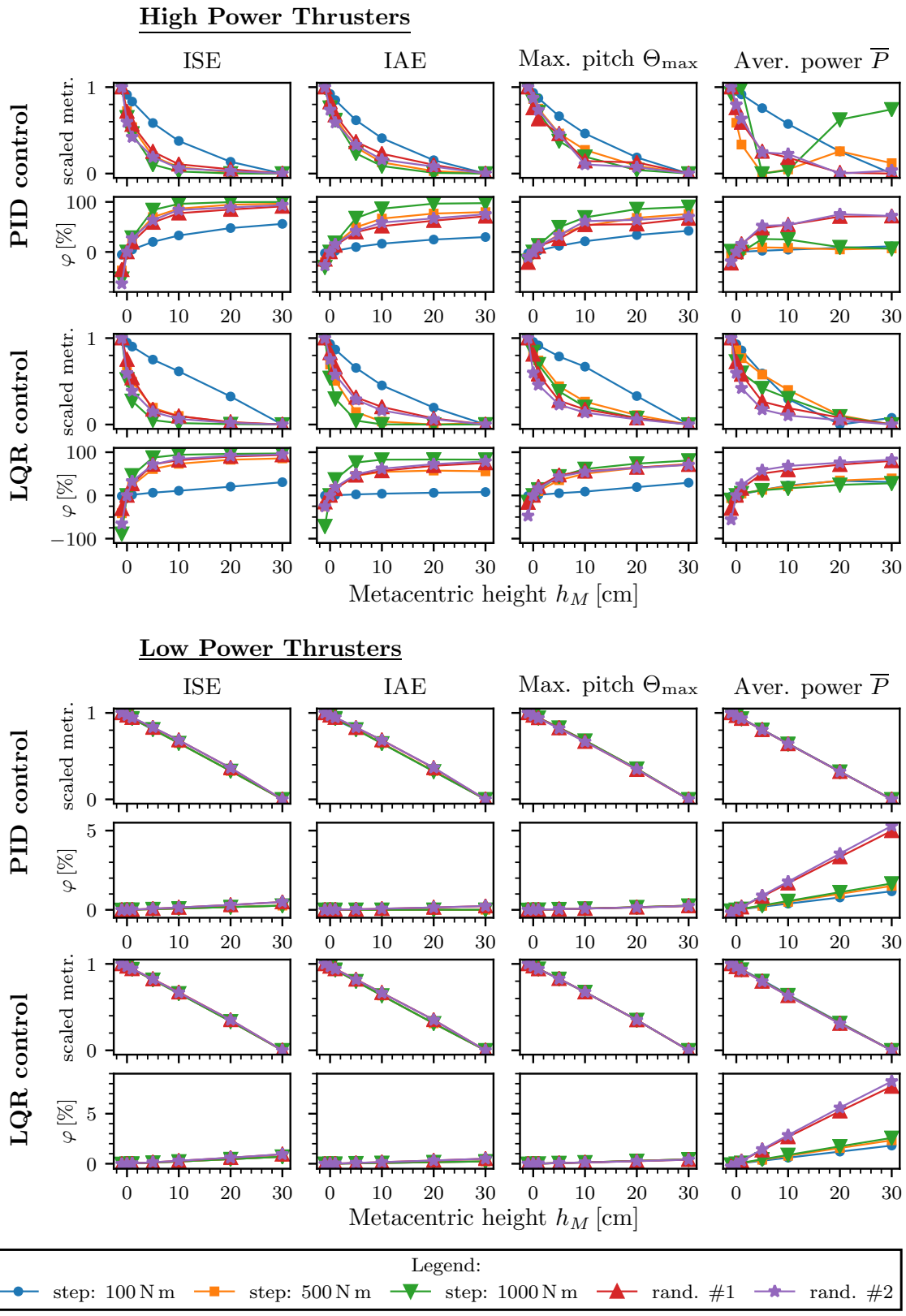

Fig. 11. Summary of simulation study results. The metrics Integral of Squared Error (ISE), Integral of Absolute Error (IAE), maximum absolute pitch angle $\Theta_{\max}$ and average power $\overline{P}$ are shown versus metacentric height for various disturbances (step and random). Metric values were scaled to make trends in data comparable among disturbances. The savings φ describe the relative improvement of metrics compared to the marginally stable configuration. Results and thus improvements strongly depend on thruster dynamics and for the HP thrusters a saturation effect can be observed.

$h_M = 30\,\mathrm{cm}$) compared to $\Theta_{\max} = 0.8°$ for the LP thrusters (at $h_M = -1\,\mathrm{cm}$).

The trend in dependence on hydrostatic stability was similar for PID and LQR control. However, there was an exception in the results for average power of PID control using the HP thrusters: energy consumption tended to increase for larger disturbances. This effect could be traced back to the accumulation of potential energy, which increased with enlarging metacentric height. Due to the relatively slow thruster response, the vehicle at first behaved as if it was not actuated and started to swing about its open loop equilibrium point. This led to oscillations in the velocity control loop, causing an increase in energy consumption. A similar behavior was observed for LQR control but less intense.

IV. Discussion

Our work set out with the aim of assessing the importance of hydrostatic stability for attitude control of I-AUVs. In section II, we found that hydrostatic stability is not strictly necessary to achieve stable pitch control. A note of caution is due here since the effects of thruster dynamics and actuator limits were neglected in the analysis. However, the controllers we presented in section III-D performed adequately throughout our simulations despite the modeled thruster behavior. We are therefore confident that suitably stable control algorithms can be found for operation of marginally stable vehicles in reality.

Concerning control performance and energy consumption, our key finding was that the influence of hydrostatic stability is strongly dependent on thruster dynamics. This result is plausible, because fast thruster dynamics allow for quicker response to disturbances. Consequently, deflections are smaller and therefore the restoring forces have less effect on vehicle motion (see (13)).

While we observed a general trend of performance improving through raising of hydrostatic stability, results were different for energy consumption of PID control in combination with HP thrusters. This exception emphasizes a bias of our analysis: results are dependent on the chosen set of simulation parameters, especially on controller choice. Use of other control algorithms may lead to substantially different outcome. Further limitations include the fact that only one DOF was considered, neglecting any coupling effects. Another source of uncertainty is the fidelity of our simulation model. Therefore, further experiments incorporating coupling are desirable—preferably in real world. Another interesting topic for future work is the influence of vehicle dynamics. In our study we considered a vehicle the size of *Cuttlefish*. It remains unclear if our conclusions are also valid for smaller vehicles.

Assuming our findings can be generalized to real world scenarios, our results suggest that operation of larger-sized, box-shaped I-AUVs is feasible if the thrusters provide a sufficiently high dynamic range. Depending on particular mission requirements, fast thruster dynamics may even be necessary to achieve adequate control performance, irrespective of hydrostatic stability considerations.

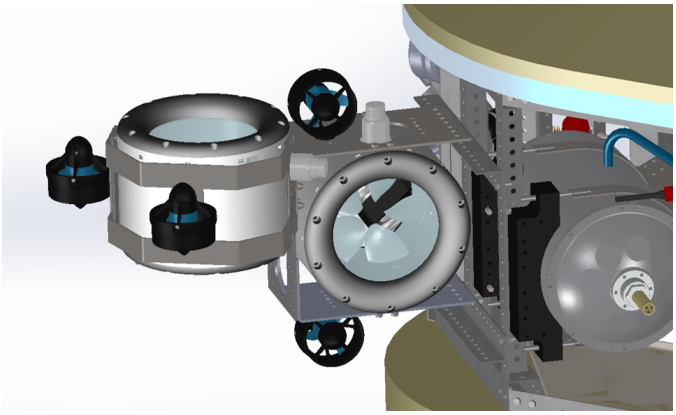

Fig. 12. Combination of thrusters with different power capabilities and response times. (CAD: DFKI)

The call for fast thruster dynamics is generally in conflict with the high power demands of large-sized vehicles, leading to huge thruster designs suffering from high rotor inertia. As a solution approach, we propose a multi-thruster configuration as illustrated in Fig. 12. By combining a high power thruster with one or more fast low power devices, high thrust capability could be merged with fast response to disturbances. We consider the efficient control of such a configuration as a promising field for future research.

V. Conclusion

In this paper, we addressed the question if hydrostatic stability can be sacrificed for I-AUVs in favor of improved agility in attitude control. We investigated the impact of hydrostatics on stability of pitch control and examined the influence of hydrostatic stability on control performance and energy consumption. Our results suggest the following conclusions:

1) To achieve stable attitude control, the vehicle does not necessarily need to be hydrostatically stable.
2) Fast thruster dynamics are desirable to improve control performance.
3) If thrusters with comparatively slow response are used, increasing hydrostatic stability substantially improves performance. However, this effect saturates for larger metacentric heights and peculiarities of the controller may have to be considered.
4) Concerning our primary research question, operation of marginally stable, larger-sized I-AUVs is feasible if the thrusters provide sufficiently high dynamic range.

As a solution to the high power vs. fast dynamics conflict in thruster design, we proposed a multi-thruster configuration.

Most current state-of-the-art I-AUVs are practically tied to a more or less fixed attitude in pitch and roll. Our results indicate that these constraints can be overcome in the future by marginally stable vehicles, expanding intervention capabilities through high agility.

TABLE III
VEHICLE MODEL PARAMETERS

Parameter	Unit	Value
m	[kg]	1200
I_y	[kg m^2]	670
$X_{\dot{u}}$	[kg]	-5968
$Z_{\dot{w}}$	[kg]	-23221
$M_{\dot{q}}$	[kg m^2]	-1578
X_u	[kg s^{-1}]	-69
Z_w	[kg s^{-1}]	-200
M_q	[kg m^2 s^{-1}]	-187
$X_{\lvert u\rvert u}$	[kg m^{-1}]	-685
$Z_{\lvert w\rvert w}$	[kg m^{-1}]	-2003
$M_{\lvert q\rvert q}$	[kg m^2]	-1866
x_b	[cm]	0
x_g	[cm]	0
z_b	[cm]	0

TABLE IV
THRUSTER MODEL PARAMETERS

Parameter	Unit	High power thruster	Low power thruster
P	[kg m^2]	1	0.5
I	[kg m^2 s^{-1}]	0.5	10
$\tau_{\min}$	[N m]	-4.75	-3800
$\tau_{\max}$	[N m]	4.75	4200
C_t	[kg m]	0.6	0.000383
α	[$-$]	0.005	0.026
β	[kg^{-1} m^{-2}]	1	1
Update rate	[Hz]	10	50

APPENDIX
SIMULATION PARAMETERS

Vehicle model parameters are given in Table III and thruster model parameters are shown in Table IV. Tables V and VI summarize the parameters used for PID and LQR based pitch control, respectively.

In Table IV, the values for the shaft torque limits $\tau_{\min}$ and $\tau_{\max}$ may appear unreasonable. This is because the parameter β, which may be interpreted as the reciprocal of propeller inertia, was set to one, for simplicity reasons.

TABLE V
PID CONTROL PARAMETERS

Parameter	HP thrusters	LP thrusters
Outer control loop (attitude)		
P_{outer}	0.4	2.5
I_{outer}	0.1	0.25
D_{outer}	0.3	–
N_{outer}	100	–
output saturation (outer)	± 0.15	± 0.3
Inner control loop (angular velocity)		
P_{inner}	3	10
I_{inner}	0.05	–
D_{inner}	0.75	–
N_{inner}	100	–
output saturation (inner)	± 0.15	± 0.3

TABLE VI
LQR CONTROL PARAMETERS

Parameter	HP thrusters	LP thrusters
P	0.08	2
Q_i	0.0886	5.0118
F_1	-0.3772	-8.256
F_2	-1.1356	-8.4055
integrator boundaries	± 5	± 200

REFERENCES

[1] P. Ridao, M. Carreras, D. Ribas, P. J. Sanz, and G. Oliver, "Intervention AUVs: The next challenge," pp. 227–241, jan 2015, in: Annual Reviews in Control.

[2] D. Ribas, N. Palomeras, P. Ridao, M. Carreras, and A. Mallios, "Girona 500 AUV: From survey to intervention," pp. 46–53, feb 2012, in: IEEE/ASME Transactions on Mechatronics, vol. 17, p. 46–53.

[3] C. Eriksen, T. Osse, R. Light, T. Wen, T. Lehman, P. Sabin, J. Ballard, and A. Chiodi, "Seaglider: a long-range autonomous underwater vehicle for oceanographic research," *IEEE Journal of Oceanic Engineering*, vol. 26, no. 4, pp. 424–436, 2001.

[4] S. Bhat and I. Stenius, "Hydrobatics: A Review of Trends, Challenges and Opportunities for Efficient and Agile Underactuated AUVs," in *AUV 2018 - 2018 IEEE/OES Autonomous Underwater Vehicle Workshop, Proceedings*. Institute of Electrical and Electronics Engineers Inc., nov 2018.

[5] A. Hackbarth, E. Kreuzer, and E. Solowjow, "HippoCampus: A micro underwater vehicle for swarm applications," in *IEEE International Conference on Intelligent Robots and Systems*, vol. 2015-Decem. Institute of Electrical and Electronics Engineers Inc., dec 2015, pp. 2258–2263.

[6] A. Mazumdar and H. H. Asada, "Control-configured design of spheroidal, appendage-free, underwater vehicles," *IEEE Transactions on Robotics*, vol. 30, no. 2, pp. 448–460, 2014.

[7] Ocean Modules Sweden AB, "ROV System Specification Comparison," http://www.ocean-modules.com/downloads/documents/Ocean-Modules-ROV-System-Specification-Comparison.pdf, online; accessed August 23, 2022.

[8] L. Christensen, J. Hilljegerdes, M. Zipper, A. Kolesnikov, B. Hülsen, C. E. S. Koch, L. C. Danter, and S. Planthaber, "The hydrobatic dual-arm intervention auv cuttlefish," in *OCEANS 2022 - Hampton Roads*, 2022, to be published.

[9] N. E. Leonard, "Stability of a bottom-heavy underwater vehicle," *Automatica*, vol. 33, no. 3, pp. 331–346, 1997.

[10] L. Miller, S. Brizzolara, and D. J. Stilwell, "Increase in stability of an x-configured auv through hydrodynamic design iterations with the definition of a new stability index to include effect of gravity," *Journal of Marine Science and Engineering*, vol. 9, no. 9, 2021.

[11] H. Zhang, J. Zhang, Y. Liu, Y. Wang, S. Wang, Z. Wu, F. Wang, L. Hao, and Y. Zheng, "Research on the influence of balance weight parameters on the motion performance of the seafloor mapping auv in vertical plane," *Ocean Engineering*, vol. 109, pp. 217–225, 2015.

[12] T. I. Fossen, *Handbook of marine craft hydrodynamics and motion control*. Chichester: Wiley, a John Wiley & Sons, Ltd., Publication, 2011.

[13] N. A. Chaturvedi, A. K. Sanyal, and N. H. McClamroch, "Rigid-body attitude control," *IEEE Control Systems Magazine*, vol. 31, no. 3, pp. 30–51, 2011.

[14] T. Rossol, "Influence of hydrostatic stability on orientation control of autonomous underwater vehicles," Master's thesis, University of Bremen, Feb. 2022. [Online]. Available: https://www.researchgate.net/profile/Tobias-Rossol/publication/363156981_Influence_of_Hydrostatic_Stability_on_Orientation_Control_of_Autonomous_Underwater_Vehicles/links/630f98ba1ddd447021235ae2/Influence-of-Hydrostatic-Stability-on-Orientation-Control-of-Autonomous-Underwater-Vehicles.pdf

[15] Blue Robotics Inc, "T200 Thruster for ROVs, AUVs, and marine robotics," https://bluerobotics.com/store/thrusters/t100-t200-thrusters/t200-thruster-r2-rp/, online; accessed on November 23, 2021.

[16] TSL Technology Ltd., "IntegratedThruster Data," http://www.tsltechnology.com/marine/thrusters_data.htm, online; accessed on August 23, 2022.

[17] D. R. Yoerger, J. G. Cooke, and J. J. E. Slotine, "The Influence of Thruster Dynamics on Underwater Vehicle Behavior and Their Incorporation Into Control System Design," *IEEE Journal of Oceanic Engineering*, vol. 15, no. 3, pp. 167–178, 1990.